PERGAMON

Polyhedron 20 (2001) 1479–1488

POLYHEDRON

www.elsevier.nl/locate/poly

Magnetization tunneling in single-molecule magnets

David N. Hendrickson [a,*], George Christou [b], Hidehiko Ishimoto [c], Jae Yoo [a], Euan K. Brechin [b], Akira Yamaguchi [c], Evan M. Rumberger [a], Sheila M.J. Aubin [a], Ziming Sun [a], Guillem Aromí [b]

[a] *Department of Chemistry and Biochemistry-0358, University of California at San Diego, La Jolla, CA 92093-0358, USA*
[b] *Department of Chemistry, Indiana University, Bloomington, Indiana, IN 47405, USA*
[c] *Institute for Solid State Physics, University of Tokyo, 7-22-1 Roppongi, Minatoku, Tokyo 106-8666, Japan*

Received 17 September 2000; accepted 13 November 2000

Abstract

The quantum mechanical tunneling of the direction of magnetization is discussed for several examples of single-molecules magnets (SMM's). SMM's are molecules that function as nanomagnets. Magnetization tunneling is described for two crystallographically different forms of $[Mn_{12}O_{12}(O_2CC_6H_4\text{-}p\text{-}Me)_{16}(H_2O)_4]$ solvate. The two Mn_{12} complexes are isomers that both differ in the positioning of the H_2O and carboxylate ligands and also in the orientations of the Jahn–Teller elongation at the Mn^{III} ions. The magnetization versus magnetic field hysteresis loop is quite different for the two isomeric Mn_{12} complexes. One Mn_{12} complex exhibits a magnetization hysteresis loop that is characteristic of considerably faster magnetization tunneling than in the other Mn_{12} isomer. The lower symmetry and greater rhombic zero-field splitting are the origin of the faster magnetization tunneling. Frequency-dependent ac magnetic susceptibility and dc magnetization decay data are presented to characterize the magnetization relaxation rate versus temperature responses of three mixed-valence Mn_4 complexes. In all three cases, the Arrhenius plot of the logarithm of the magnetization relaxation rate versus the inverse absolute temperature shows a temperature-dependent region as well as a temperature-independent region. The temperature-independent magnetization rate is definitive evidence of magnetization tunneling in the lowest-energy zero-field component of the ground state.

Keywords: Nanomagnet; Single-molecule magnet; Magnetization tunneling; Superparamagnet

1. Introduction

In 1993 it was discovered that $[Mn_{12}O_{12}(O_2CMe)_{16}(H_2O)_4]\cdot 4H_2O\cdot 2MeCOOH$ (**1**) functions as a nanoscale magnet [1,2]. Such a molecule has been called [3] a single-molecule magnet (SMM). There has been considerable interest in the magnetic properties of complex **1** [4–22], which has a $S = 10$ ground state split by axial zero-field splitting (DS_z^2, where $D = -0.5$ cm^{-1}). In 1996, it was reported [23–26] that complex **1** exhibits quantum mechanical tunneling of the direction of magnetization.

The number of known single-molecule magnets is limited. Polynuclear metal complexes with the composition $Mn_4^{IV}Mn_8^{III}$, $Mn_4^{IV}Mn_7^{III}Mn_1^{II}$, $Mn^{IV}Mn_3^{III}$, Mn_2^{III}-Mn_2^{II}, V_4^{III}, Fe_8^{III}, and Fe_4^{III}, have been shown [4,5] to function as SMM's. Relative to classical nanomagnets prepared perhaps by fragmentation of macroscopic multi-domain particles, single-molecule nanomagnets offer several advantages. First, SMM's are prepared by a solution method and, once purified, are composed of single, sharply defined sizes and not a distribution of particle sizes. Second, SMM's are readily amenable to many systematic changes, such as changing the peripheral ligands or overall oxidation state of the molecule. Third, SMM's can be made to be soluble in a wide range of solvents. This could, for example, facilitate the preparation of films of SMM's. Fourth, since each SMM has sub-nanoscale dimensions, they could be used as high-density memory devices or even in quantum computers. Fifth, understanding the magnetic properties of SMM's could prove important to help bridge the gap between the quantum and classical understanding of magnetism.

* Corresponding author. Present address: Chemistry Department, University of California, La Jolla, CA 92093-0506, USA.
E-mail address: dhendrickson@ucsd.edu (D.N. Hendrickson).

0277-5387/01/$ - see front matter
PII: S0277-5387(01)00639-8

Each SMM functions as a superparamagnet as a result of having a large-spin ground state with appreciable magnetoanisotropy. The source of the magnetoanisotropy is single-ion zero-field interactions that are present at individual metal ions in one molecule. At temperatures below the 'blocking temperature' the magnetic moment of a SMM changes sluggishly from 'spin up' to 'spin down'. As a result of this slow magnetization relaxation, SMM's exhibit: (1) magnetization hysteresis loops; (2) frequency-dependent out-of-phase ac magnetic susceptibility signals and (3) slow magnetization decay after an external magnetic field is removed when the temperature is below the blocking temperature. It is important to emphasize that the SMM phenomenon arises from the behavior of individual isolated molecules.

A SMM has a potential-energy barrier for reversal of its magnetic moment. It has been found that, in addition to thermal activation of each SMM over the barrier, the reversal of the direction of magnetization also occurs via quantum mechanical tunneling through the barrier [27]. In this paper we will discuss some recent observations on SMM's that are manifestations of magnetization tunneling.

2. Experimental

2.1. Materials

All chemicals and solvents were used as received. All preparations and manipulations were performed under aerobic conditions. $(N^nBu_4)[MnO_4]$ was prepared as described in Ref. [26].

2.2. Warnings

Organic permanganates should be handled with extreme caution. Detonation of some organic permanganates have been reported [28] while drying at high temperatures.

2.3. $[Mn_{12}O_{12}(O_2CC_6H_4\text{-}p\text{-}Me)_{16}(H_2O)_4]\cdot HO_2CC_6H_4\text{-}p\text{-}Me$ (Complex **2**)

$Mn(ClO_4)_2$ (4.00 g, 11.0 mmol) was dissolved in 100% ethanol (20 ml) followed by the addition of *p*-methylbenzoic acid (19.13 g, 140.5 mmol) and additional ethanol (180 ml). $(N^nBu_4)[MnO_4]$ (1.55 g, 4.28 mmol) was slowly added followed by filtration. The reddish–brown filtrate was left uncapped and undisturbed for 2 weeks. The resulting brown solid $[Mn_{12}O_{12}(O_2CC_6H_4\text{-}p\text{-}Me)_{16}(H_2O)_4]$ (7% yield based on Mn) was collected on a frit, washed with 100% ethanol, and recrystallized from CH_2Cl_2 hexanes, yielding black needles. Later it was discovered that higher yields (20%) were obtained if the synthesis was done in 2% H_2O:98% ethanol. The resulting microcrystals were washed with 100% ethanol and dried under vacuum. Recrystallization from anhydrous CH_2Cl_2:hexane lead to black microcrystals. Anal. Calc. (Found) for $C_{136}H_{128}O_{50}Mn_{12}$: C, 50.70 (50.78); H, 4.00 (3.94)%.

2.4. $[Mn_{12}O_{12}(O_2CC_6H_4\text{-}p\text{-}Me)_{16}(H_2O_4]\cdot 3H_2O$ (Complex **3**)

This complex was prepared in an analogous fashion as for complex **2**, except instead of 100% ethanol, a 20% H_2O:80% ethanol solution (260 ml) was used. The yield based on total available Mn was 9%. Anal. Calc. (Found) for $C_{130}H_{132}O_{54}Mn_{12}$: C, 49.0 (48.9); H, 4.04 (4.12)%.

2.5. $[Mn_4(OAc)_2(pdmH)_6(H_2O)_4](ClO_4)_2$ (Complex **5**)

2.5.1. Method 1

$[Mn_3O(O_2CMe)_6(py)_3](ClO_4)$ (**7**) (0.500 g, 0.574 mmol) and $pdmH_2$ (0.240 g, 1.72 mmol) were dissolved in CH_2Cl_2 (30 ml) and the resultant red–brown solution was stirred overnight at room temperature (r.t.). During this time, a fine brown precipitate slowly formed, and this was collected by filtration, washed with a little CH_2Cl_2, redissolved in MeCN (20 ml), and the solution filtered. The filtrate was layered with Et_2O to slowly give well-formed brown crystals. After 3 days they were collected by filtration, washed with Et_2O, and dried in vacuo. The yield was $\sim$50%. Dried solid was analyzed to be solvent-free. Anal. Calc. (Found) for $C_{46}H_{54}Cl_2Mn_4N_6O_{24}$: C, 40.42 (40.50); H, 3.95 (4.10); N, 6.15 (6.04)%. Selected IR data (cm^{-1}): 1605 (s), 1582 (s), 1464 (m), 1447 (m), 1381 (m), 1331 (m), 787 (m), 691 (m), 666 (m), 627 (m).

The crystallographic sample was maintained in contact with the mother liquor to prevent solvent loss, and it was identified crystallographically as **1**·2MeCN·Et_2O. In contact with air, complex **1** becomes hydrated to give complex **1**·2.5H_2O. Anal. Calc. (found) for $C_{46}H_{54}Cl_2Mn_4N_6O_{24}\cdot 2.5H_2O$: C, 39.12 (39.11); H, 4.04 (3.88); N, 5.95 (6.13)%.

2.5.2. Method 2

Complex **7** (0.500 g, 0.574 mmol) and $pdmH_2$ (0.240 g, 1.72 mmol) were dissolved in MeCN (30 ml) and the solution stirred overnight at r.t. No precipitate was obtained. The solution was filtered and the filtrate layered with Et_2O to give brown crystals, which were isolated after 7 days, washed with Et_2O, and dried in vacuo. The yield was 15% and the solid was spectroscopically (IR) identical with that from method 1.

2.6. $[Mn_4(hmp)_6Br_2(H_2O)_2]Br_2$ (Complex **6**)

2-Hydroxymethylpyridine (hmpH) (376 mg) and 395 mg of $MnBr_2{\cdot}4H_2O$ were dissolved in 20 ml of MeCN. To this was added 530 mg of 20% wt water solution of tetraethylammonium hydroxide. The solution turned red–brown and this was stirred for 40–60 min and then filtered. The filtrate was then left to slowly evaporate. Dark cube-like crystals of $\mathbf{6}{\cdot}4H_2O$ formed in 1–2 weeks. *Anal.* Calc. (Found) for $C_{36}H_{48}Br_4Mn_4N_6O_{12}$: C, 33.36 (33.83); H, 3.73 (3.47); N, 6.48 (6.56). Selected IR data (cm^{-1}): 3350.2 (br), 1604.7 9 (s), 1483.2 (m), 1438.8 (m), 1282.6 (w), 1226.7 (w), 1155.3 (w), 1045.4 (s), 765.7 (s), 659.6 (s), 567.1 (s).

2.7. Physical measurements

IR measurements were made on samples pressed into KBr pellets using a Nicolet model 510P spectrophotometer. Direct current magnetic susceptibility experiments were performed on powdered microcrystalline samples (restrained in eicosane to prevent torquing at high fields) on a Quantum Design MPMS superconducting quantum interference device (SQUID) magnetometer equipped with a 5.5 T (55 kG) magnet and capable of operating in the 1.7–400 K range. Diamagnetic contributions to the susceptibility were corrected using Pascal's constants.

The ac magnetic susceptibility experiments above 1.7 K were carried out on a Quantum Design MPMS2 SQUID magnetometer. The ac field strength can be varied from 0.001 to 5 G at frequencies ranging from 0.0005 to 1512 Hz. The temperature range available is 1.7–400 K. Low-temperature ac magnetic susceptibility experiments down to the millikelvin temperature range were performed at the Institute of Solid State Physics, The University of Tokyo. Measurements were made on a SHE-RLM bridge where a SQUID served as a null detector. Measurements were made on a powdered microcrystalline sample stuck on a quartz glass with a small amount of Apiezon grease to reduce the background signal. It was immersed in a nonmagnetic liquid ^4He, which was cooled by way of a sintered powder heat exchanger with a ^3He–^4He dilution refrigerator. The temperature was determined with germanium and carbon resistor thermometers. Thermal contact between the sample and the coolant was found to be good enough because the susceptibility of the sample quickly followed the temperature change of the refrigerator. Data were collected in the 1.1–995 Hz frequency range between 0.4 and 3.5 K.

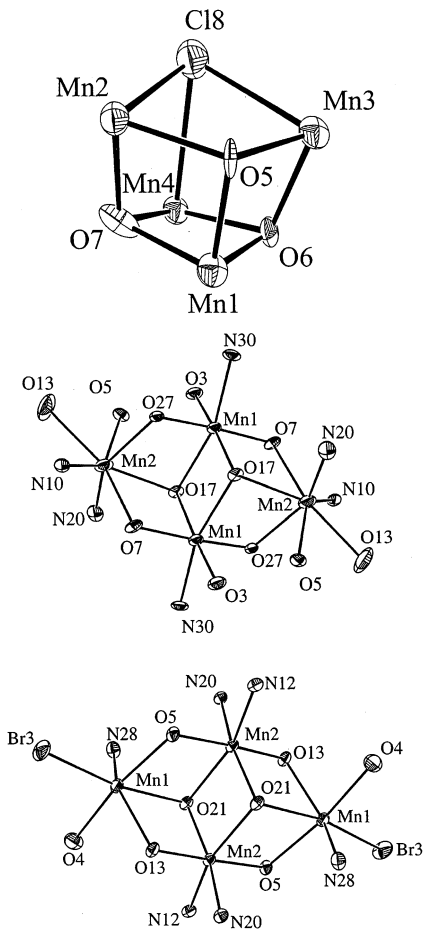

Fig. 1. Drawings of the cores of $[Mn_4O_3Cl(O_2CMe)_3(dbm)_3]$ (**4**) (top), $[Mn_4(OAc)_2(pdmH)_6(H_2O)_4](ClO_4)_2$ (**5**) (middle) and $[Mn_4(hmp)_6Br_2(H_2O)_2]Br_2{\cdot}4H_2O$ (**6**) (bottom).

3. Results and discussion

3.1. X-ray structures

The occurrence of magnetization tunneling is discussed for two $Mn_4^{IV}Mn_8^{III}$, one $Mn^{IV}Mn_3^{III}$, and two $Mn_2^{III}Mn_2^{II}$ complexes. The complexes have the following formulas:

$[Mn_{12}O_{12}(O_2CC_6H_4\text{-}p\text{-}Me)_{16}(H_2O)_4]\cdot(HO_2CC_6H_4\text{-}p\text{-}Me)$ (**2**)

$[Mn_{12}O_{12}(O_2CC_6H_4\text{-}p\text{-}Me)_{16}(H_2O)_4]{\cdot}3H_2O$ (**3**)

$[Mn_4O_3Cl(O_2CMe)_3(dbm)_3]$ (**4**)

$[Mn_4(OAc)_2(pdmH)_6(H_2O)_4][(ClO_4)_2$ (**5**)

$[Mn_4(hmp)_6Br_2(H_2O)_2]Br_2{\cdot}4H_2O$ (**6**)

The X-ray structures of complexes **4** [29] and **5** [30] have already been reported. Fig. 1 shows drawings of the core of the Mn_4 molecules in these complexes. Complex **4** has a distorted trigonal pyramidal arrangement of three Mn^{III} ions with one Mn^{IV} ion. This complex has a $S = 9/2$ ground state. In the case of $\mathbf{5}{\cdot}2MeCN{\cdot}Et_2O$, the cation sits on a planar Mn_4 rhombus that is mixed-valent $Mn_2^{III}Mn_2^{II}$. The structural parameters identify Mn(1) and Mn(2) as Mn^{III} and Mn^{II}, respectively. This solvated complex readily loses

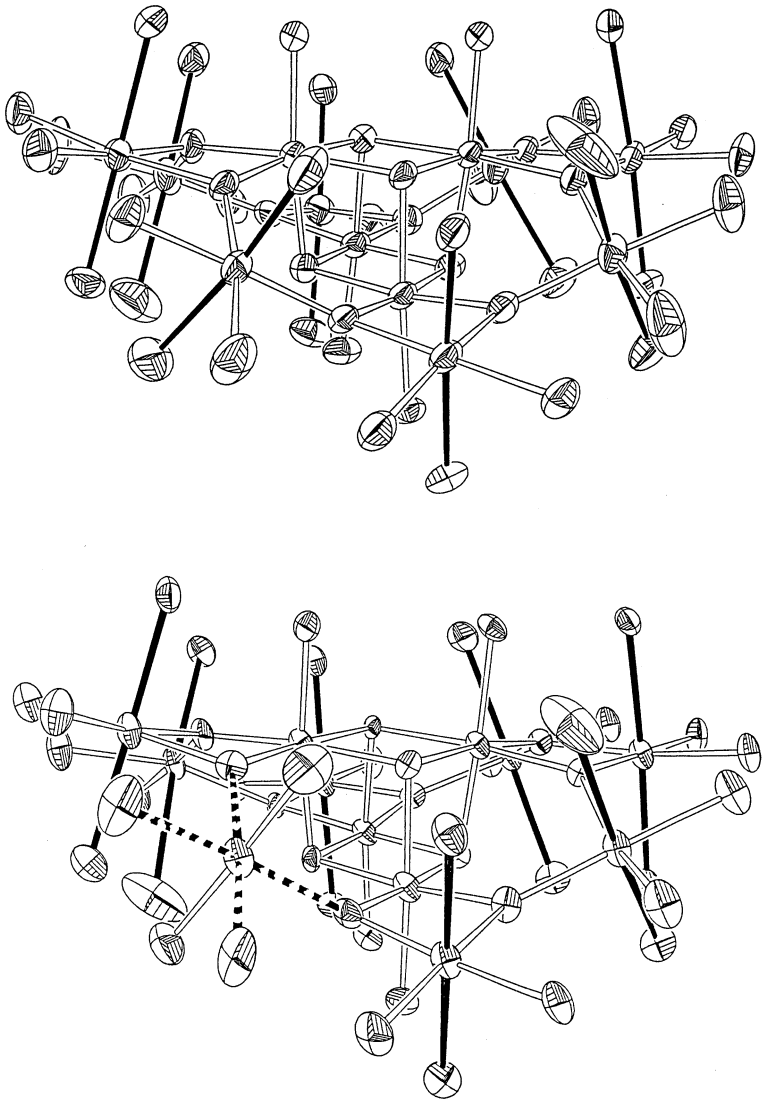

Fig. 2. ORTEP representations of the cores (i.e. without *p*-methylbenzoate ligands) of the Mn_{12} complexes in (bottom) $[Mn_{12}O_{12}(O_2CC_6H_4\text{-}p\text{-}Me)_{16}(H_2O)_4]\cdot(HO_2CC_6H_4\text{-}p\text{-}Me)$ (complex **2**) and (top) $[Mn_{12}O_{12}(O_2CC_6H_4\text{-}p\text{-}Me)_{16}(H_2O)_4]\cdot 3H_2O$ (complex **3**). Each of the eight Mn^{III} ions in a Mn_{12} complex shows a tetragonally elongated Jahn–Teller distortion. In the case of complex **3** the JT elongation axes are indicated as solid lines. For complex **2**, one JT elongation axis (dashed lines) is pointed at an O^{2-} ion and is unusual. There are two dashed lines because the molecule has a crystallographic C_2 axis disorder.

acetonitrile to give complex **5** that has been reported [30] to have a $S = 8$ ground state.

Complex **6** crystallizes in the space group $P2_1/c$ with the cation lying on an inversion center and consisting of a planar Mn_4 rhombus (see Fig. 1) [31]. The cluster is also mixed-valent with two Mn^{III} ions and two Mn^{II} ions and is structurally similar to the tetranuclear complex **5**. This complex has been found [31] to have a $S = 9$ ground state.

As shown in Fig. 2, complexes **2** and **3** have the well known $[Mn_{12}O_{12}(O_2CR)_{16}(H_2O)_4]$ structure as has been reported [2,3] previously for the benzoate ($R = -C_6H_5$) and propionate ($R = -CH_2CH_3$) complexes. As a result of the different solvate molecules in the two crystals, complex **2** crystallizes in the $C2/c$ space group, whereas complex **3** crystallizes in the $I2/a$ space group [32]. Even though both of these complexes have the same ligands on the Mn_{12} complexes, there are two significant differences in the molecular structures of the Mn_{12} molecules in **2** and **3**. First, complexes **2** and **3** differ in the positioning of the four H_2O ligands. The two Mn_{12} complexes are geometrical isomers with two different positions of the H_2O and $^{-}O_2CC_6H_4\text{-}p\text{-}Me$ ligands. Complexes **2** and **3** have one other very important difference in their structures. Each Mn^{III} ion experiences a Jahn–Teller (JT) elongation. As can be seen in Fig. 2 (top), all of the JT elongation axes in the hydrate complex **3** are roughly parallel and perpendicular to the plane of the disc-like $Mn_{12}O_{12}$ core. For complex **2** in Fig. 2 (bottom), however, it can be seen that one JT

axis is abnormally oriented; the situation is slightly complicated by the fact that the molecule has a crystallographic C_2 axis disordering the JT axis about two positions. This JT elongation axis is directed at a core O^{2-} ion and is unusual.

3.2. Potential-energy diagram and magnetization hysteresis loops

Complexes **2** and **3** have been determined [32] to have $S = 10$ ground states. As illustrated in Fig. 3 for a $S = 10$ SMM, the combination of a large spin and anisotropy leads to a potential-energy barrier for reversal of the direction of magnetization. Zero-field interactions split the $S = 10$ state into the $M_s = \pm 10$, ± 9, ± 8, ..., ± 1, 0 levels depicted in Fig. 3. The $M_s = -10$ state can be viewed as the 'spin up' state and the $M_s = +10$ state as the 'spin down' state. The double-well diagram of Fig. 3 shows how the potential energy of one molecule changes as it reverses its direction of magnetization from 'spin up' to 'spin down'. The potential-energy barrier is given as $U = |DS_z^2|$, where DS_z^2 gauges the axial zero-field splitting in the $S = 10$ ground state.

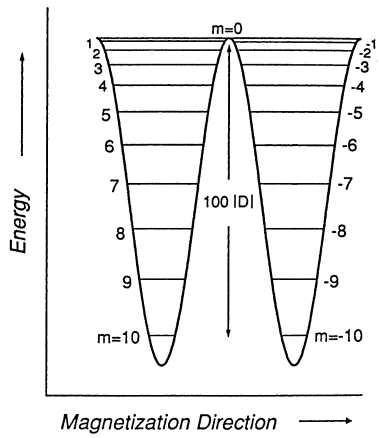

Fig. 3. Plot of potential energy versus magnetization direction for a single Mn_{12} molecule in zero applied magnetic field with a $S = 10$ ground state. There is an axial zero field splitting, characterized by $H = DS_z^2$ where $D < 0$.

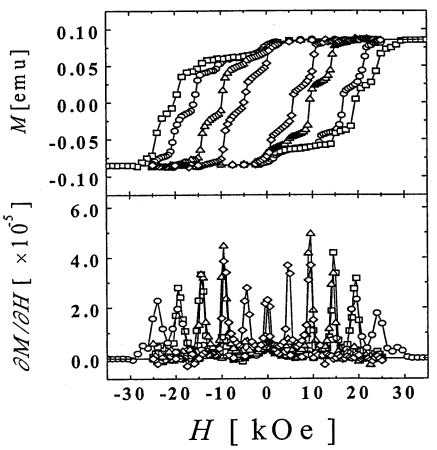

Fig. 4. Plots of magnetization versus external magnetic field for $[Mn_{12}O_{12}(O_2CC_6H_4\text{-}p\text{-}Me)_{16}(H_2O)_4]\cdot 3H_2O$ (complex **3**) at five temperatures in the 1.72–2.50 K range. Five small crystals (1.2 mg total) were oriented in a frozen eicosane matrix so that the magnetic field is parallel to the principal axis of magnetization.

Since complexes **2** and **3** have barriers for changing their magnetic moments from 'spin up' to 'spin down' (Fig. 3), it is informative to examine the change in the magnetization of a sample as an external field is changed. For an oriented sample, steps can be seen at regular intervals of magnetic field in the magnetization hysteresis loop of a SMM. These steps result from quantum mechanical tunneling of the magnetization [23–26]. Oriented samples of complexes **2** and **3** were prepared by suspending a few small crystals of either complex in an eicosane wax cube.

Fig. 4 shows the magnetization hysteresis data measured for complex **3**. Magnetization hysteresis loops are seen in the 1.72–2.50 K range. The coercive magnetic field and consequently the area enclosed within a hysteresis loop increase as the temperature is decreased. It is instructive to examine the features seen in one of these loops. At 1.72 K the eicosane cube with oriented crystallites is first exposed to a magnetic field of $+3.5$ T. In this field there is a saturation of the magnetization. In reference to Fig. 3 which shows the energetics in zero external field, a field of $+3.5$ T leads to the $M_s = -10$ level being considerably stabilized in energy relative to the $M_s = +10$ level. All molecules have their moments aligned parallel ('spin up') to the external magnetic field and are in the $M_s = -10$ state at 1.72 K. The magnetic field is then swept from 3.5 T to zero. If there was no barrier for converting from 'spin up' to 'spin down', then at zero external field there would be equal numbers of molecules with 'spin up' and 'spin down'. With no barrier the magnetization would go to zero at zero field. This is not the case, because there is a barrier. At 1.72 K the Mn_{12} molecules do not have enough thermal energy to go over the barrier. Reversal of the direction of the external field, followed by increasing the field to -3.5 T again leads to magnetization saturation. In this case the $M_s = +10$ 'spin down' state is stabilized in energy and all molecules are in the $M_s = +10$ state. The field is then cycled from -3.5 T to zero, reversed and then cycled back to $+3.5$ T. At 1.72 K the coercive magnetic field for complex **7** is ca. 2 T.

Close examination of the magnetization hysteresis loops shown in Fig. 4 for complex **3** shows that each hysteresis loop is not smooth, but steps are seen at regular intervals of the external field. These steps are due to tunneling of the magnetization. That is, a Mn_{12} molecule in the 'spin up' state can either be thermally activated over the barrier to the spin down state or it

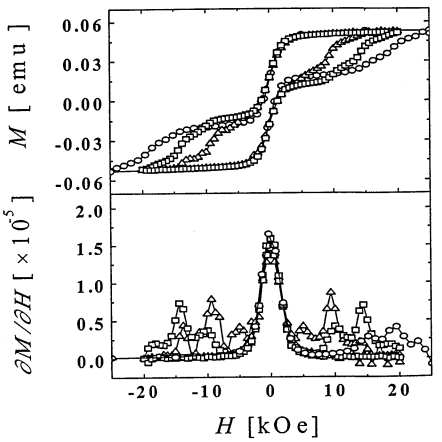

Fig. 5. Plots of magnetization versus external magnetic field for $[Mn_{12}O_{12}(O_2CC_6H_4\text{-}p\text{-}Me)_{16}(H_2O)_4]\cdot(HO_2CC_6H_4\text{-}p\text{-}Me)$ (complex **2**) at five temperatures in the 1.72–2.20 K range. Six small crystals (2.2 mg) were oriented in a frozen eicosane matrix so that the external magnetic field is parallel to the principal axis of magnetization.

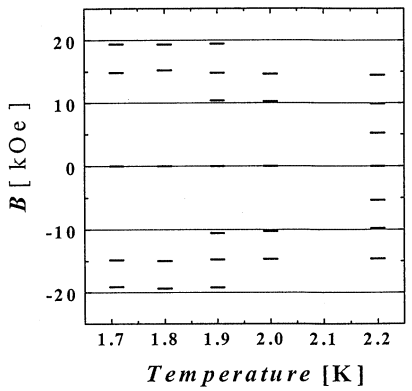

Fig. 6. Plot of the magnetic induction B versus temperature for complex **2**. Two magnetic induction (B) values were calculated from $B = H + 4\pi M$, with the external field (H) values obtained from the peak positions determined in the first-derivative magnetization plots.

reverses its direction of magnetization by tunneling through the barrier. These steps are clear evidence of tunneling of magnetization [23–26], which can be understood in the following manner. After saturation in a $+3.5$ T field, the external field about the crystallites of complex **3** is reduced to zero (Fig. 1) and at this instant all of the molecules are in the $M_s = -10$ state. Depending on the rate of sweep of the external field, some of the molecules may tunnel from the $M_s = -10$ to the $M_s = +10$ state, or more generally from the $M_s = -n$ to the $M_s = +n$ state ($n = 10, 9, 8, \ldots, 1$). Thus, at zero field we see the first step. Reversal of the external field, followed by changing the field from zero to ~ -0.48 T leads to the appearance of a second step at $H = -0.48$ T. At this external field the $M_s = -10$ state has the same energy as the $M_s = +9$ state. The alignment of energy levels leads to resonant magnetization tunneling. In this way, as the field is swept from zero to -3.5 T, steps are seen at regular intervals of ~ 0.48 T. No steps are seen as the field is swept from $+3.5$ T toward zero. Only when the field is zero, do we see the first step on the reverse sweep. The second field reversal leads to regular steps as the field is swept from zero to $+3.5$ T.

Magnetization hysteresis loops were measured for the oriented eicosane cube of complex **2** at temperatures of 1.72, 2.20, 2.00, 1.90 and 1.80 K, (Fig. 5). The hysteresis loops for complex **2** look quite different from those for complex **3**. When the external field is reduced from $+2.5$ T to zero, the magnetization falls off dramatically. The coercive fields are considerably less for complex **2** than for complex **3**. These two p-methylbenzoate Mn_{12} complexes experience quite different kinetic barriers for reversal of magnetization. It must be emphasized that the sweep rate for all the loops was 25 Oe s^{-1}. First derivative plots were calculated for each of the hysteresis loops. (lower plots in Figs. 4 and 5).

A careful analysis of the hysteresis data for complex **2** shows that the external field for each step does shift slightly with temperature. Friedman et al. [23,25] confirmed that the small shift is due to the fact that each Mn_{12} molecule does not just experience the applied field (H) but rather it experiences a magnetic induction (B) due to combination of the external field and dipolar fields from neighboring molecules in the crystal. The magnetic induction B is given as $B = H + 4\pi M$ and is invariant for each step. Fig. 6 gives a plot of magnetic induction versus the temperature for the five hysteresis loops measured for complex **2**. It can be seen that the steps determined at different temperatures have essentially the same magnitude of increment in magnetic induction. In this way the increment was found to be 0.47 T for complex **2**, and 0.48 T for complex **3.**

From the hysteresis loop data it is clear that the p-methylbenzoate complex **2** has an appreciably greater rate of magnetization relaxation than does isomeric complex **3**. This can be quantified by analyzing the frequency dependencies of the χ''_M signals for the two complexes reported previously [32]. Ac susceptibility data were collected at eight different frequencies from 1.0 to 1512 Hz for complex **3**. From the peaks in the χ''_M versus temperature plots values of the magnetization relaxation time τ were determined at eight temperatures. These data gives a straight line Arrhenius plot of $\ln(1/\tau)$ versus the inverse absolute temperature ($1/T$) for complex **3**. The data was least-squares fit to the Arrhenius eqn (Eq. (1)) to give the parameters of $\tau_0 = 7.7 \times 10^{-9}$ s and $U_{eff} = 64$ K. A similar analysis of the frequency dependence of the dominant low temperature χ''_M peak in the ac data for complex **2** gives $\tau_0 = 2.0 \times 10^{-10}$ s and $U_{eff} = 38$ K. The activation energy (U_{eff}) for reversal of the direction of the magnetization for complex **2** ($U_{eff} = 38$ K) is considerably less than that ($U_{eff} = 64$ K) for the isomeric complex **3**. The Mn_{12}-acetate complex **1** has been reported [9] to have a

U_{eff} value of 62 K, very close to the value for complex **3**.

$$\tau = \tau_0 \exp(U_{eff}/kT) \quad (1)$$

It is likely that the appreciably faster rate of magnetization tunneling observed for complex **2** compared to the isomeric complex **3** is due to the lower symmetry observed for complex **2**. This lowered symmetry would increase the rhombic zero-field splitting $[E(S_x^2 - S_y^2)]$ in the $S = 10$ ground state of complex **2** leading to an increase in the rate of magnetization tunneling. The importance of rhombicity in tunneling can be understood in the next section.

3.3. Mechanism of resonant magnetization tunneling

Chudnovsky et al. [33] have discussed the mechanism of resonant magnetization tunneling for a SMM such as complex **1**. It was assumed that the magnetization tunneling occurs as a result of a transverse magnetic field and the rates of tunneling between pairs of $+M_s$ and $-M_s$ states were calculated. It was concluded that the rate of tunneling for the $M_s = -10$ to $M_s = +10$ conversion (see Fig. 3) of a $S = 10$ molecule occurs with a lifetime longer than the universe when the transverse magnetic field is small. The rate calculated for the $M_s = -3$ to $M_s = +3$ tunneling was found to be close to the experimental value. It was suggested that at low temperatures, where steps are seen on hysteresis loops, an individual molecule is excited by a phonon in an Orbach process from the $M_s = -10$ level successively to the $M_s = -9.$, -8, -7, -6, -5, -4, and finally the $M_s = -3$ level. After it is excited to the $M_s = -3$ level, the Mn_{12} molecule then tunnels to the $M_s = +3$ level. A single tunneling channel ($M_s = -3$ to $M_s = +3$) would be opened up and this gives the first step at a zero external field in the hysteresis loop.

In addition to a transverse magnetic field, it has now been shown [34] that other interactions, such as a transverse quartic zero-field interaction, are probably also important in influencing the rate of magnetization tunneling in complex **1**. For each Mn_{12} molecule the spin Hamiltonian given in Eq. (2) applies:

$$H = H_A + H_z + H_{sp} + H_T \quad (2)$$

The first term H_A is for the axial (longitudinal) zero-field interactions, the leading terms of which are given as

$$H_A = DS_z^2 - FS_z^4 \quad (3)$$

The parameter D is considerably larger than F and gauges the second-order axial zero-field splitting. The second term in Eq. (2), H_z, is just the Zeeman term, which in its simplest form is given in Eq. (4).

$$H_z = g\mu_B H_z S_z \quad (4)$$

The term H_{sp} represents the spin-phonon coupling, where a given Mn_{12} complex interacts with phonons in the crystal. The last term H_T, representing transverse interactions, is the most important in terms of the rate of magnetization tunneling. Some of the larger terms in H_T are given in Eq. (5):

$$H_T = g\mu_B H_x S_x + E(S_x^2 - S_y^2) - G(S_+^4 + S_-^4) \quad (5)$$

The raising and lowering operators are given as $S_\pm = S_x \pm iS_y$. The transverse magnetic field H_x, or the rhombic zero-field operator $(S_x^2 - S_y^2)$ or the quartic zero-field operator $(S_+^4 + S_-^4)$ mix together the M_s wavefunctions and this facilitates tunneling of the magnetization. There is still considerable research needed to understand this tunneling phenomenon [35].

The Mn_{12}-acetate complex **1** is excited by phonons to an $M_s = -3$ tunneling channel. Tunneling of the magnetization in the ground state levels ($M_s = \pm 10$) has not been observed for complex **1**. Tunneling from the lowest energy level has been observed for a few SMM's.

3.4. Temperature-independent magnetization tunneling in complex 4

In 1998 we reported [29] the presence of temperature-independent magnetization in the $Mn^{IV}Mn_3^{III}$ complex **4**. The complex $[Mn_4O_3Cl(O_2CMe)_3(dbm)_3]$ (**4**) where dbm^- is the monoanion of dibenzoylmethane, has an $S = 9/2$ ground state [29]. Since complex **4** shows frequency-dependent out-of-phase ac susceptibility signals and magnetization hysteresis loops below 0.90 K, this complex is a SMM. Steps are seen on each hysteresis loop. An Arrhenius plot of the magnetization relaxation data for complex **4** indicates a thermally activated region between 2.0 and 0.70 K and a temperature-independent region at temperatures below 0.70 K. A fit of the data in the temperature-dependent region gives $U_{eff} = 11.8$ K and $\tau_0 = 3.6 \times 10^{-7}$ s. With the D value obtained from HFEPR data for this $S = 9/2$ complex **4**, U can be calculated as 15.2 K ($= 10.6$ cm^{-1}). It was concluded that the temperature-independent magnetization relaxation must correspond to magnetization tunneling between the lowest degenerate levels, the $M_s = 9/2$ and $-9/2$ levels for the $S = 9/2$ complex **4**. A temperature-independent magnetization relaxation below 0.35 K has also been reported for a Fe_8^{III} complex that has a $S = 10$ ground state [36]. This Fe_8^{III} complex has been found to have $U_{eff} = 24.5$ K and zero-field interaction parameters of $D = -0.27$ K and $E = -0.046$ K. Tunneling in the lowest energy $M_s = \pm 10$ levels is seen for this Fe_8^{III} complex.

It is important to note that Mn_4 complex **4** and the Fe_8 complex show tunneling in the lowest-energy level because they possess relatively large transverse interactions, i.e. terms in Eq. (5). Due to its crystal site

symmetry the Mn_{12}-acetate complex **1** has no rhombic zero-field splitting, and $E = 0$. Complex **4** and the Fe_8^{III} complex probably show tunneling in the lowest-energy levels because each of these complexes is of lower symmetry and this gives a non-zero E value.

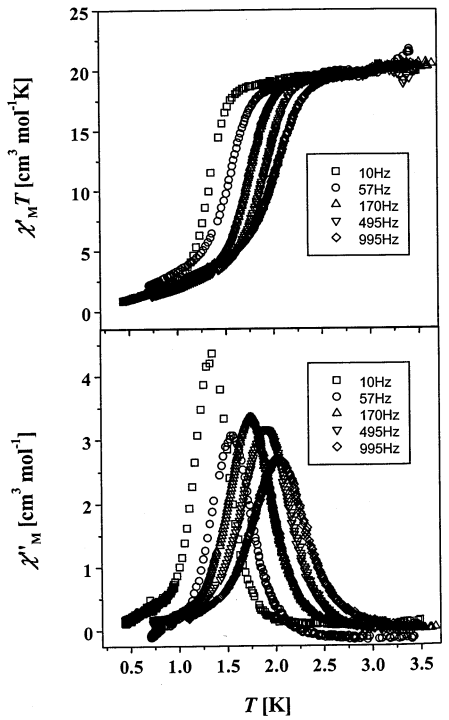

Fig. 7. Plots of χ'_M (top) and χ''_M (bottom) versus temperature for a polycrystalline sample of complex **5** in a 1.0 G ac field oscillating at the indicated frequencies, where χ'_M and χ''_M are the in-phase and out-of-phase ac magnetic susceptibilities, respectively.

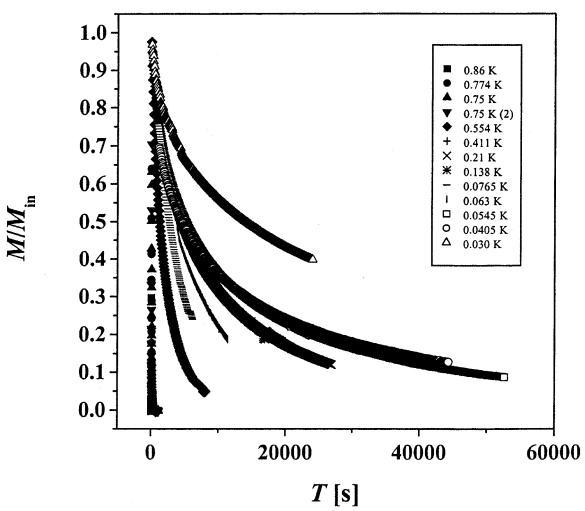

Fig. 8. Dc magnetization decay as a function of time at the indicated temperatures for complex **5**.

3.5. Magnetization tunneling in the Mn_4 complexes **5** and **6**

Variable-field magnetization data have been fit [30] to determine that complex **5** has a $S = 8$ ground state with $D/k_B = -0.358$ K. Ac magnetic susceptibility measurements have been carried out by cooling the sample with a ^3He–^4He dilution refrigerator in the 0.4–3.5 K range. Eleven different ac frequencies were used (Fig. 7 shows data taken at five different frequencies) in the 1.1–995 Hz range, which gave rates of magnetization reversal at eleven different temperatures. These relaxation data fit well to the Arrhenius equation to give an activation energy for magnetization reversal of $U_{eff} = 17.3$ K with a preexponential factor of $\tau_0 = 2.54 \times 10^{-7}$ s. The thermodynamic barrier can be calculated to be $U = 22.4$ K. As with other SMMs, it is expected that $U > U_{eff}$, for the reversal of magnetization not only involves a thermal activation over the potential-energy barrier, but also quantum tunneling of the direction of magnetization.

The most definitive data showing that complex **5** does reverse its magnetization direction by quantum tunneling were obtained by means of magnetization decay experiments. In a dc magnetization decay experiment the sample is first cooled and maintained at a low temperature, after which it is subjected to a very small magnetic field. At low temperatures, only a small field is needed to achieve magnetization saturation. The field is then suddenly removed and the magnetization is measured as a function of time. Over time the magnetization decays from some initial value at time zero, defined as the time when the applied field becomes zero, to an equilibrium value.

Fig. 8 shows magnetization decay data for complex **5** employing a small dc magnetic field of 3.7 Oe. Plots of magnetization versus time are given in the 0.030–0.860 K range. These magnetization decay data were fit to a stretched exponential function. This gave a set of relaxation times at temperatures in the 0.030–0.860 K range. It was found that at temperatures above ~ 0.5 K the magnetization relaxation time τ is temperature dependent.

The magnetization rate data obtained at higher temperatures for complex **5** with ac susceptibility measurements are combined with the dc magnetization decay rate data as an Arrhenius plot of ln $(1/\tau)$ versus $1/T$ in Fig. 9. This is indeed a very revealing plot for it can be seen that at temperatures above ~ 0.5 K, the magnetization relaxation rate is temperature dependent with an activation energy of $U_{eff} = 17.3$ K. However, at low temperatures (below ~ 0.5 K) the relaxation rate is clearly temperature independent, indicating that the magnetization relaxation below this temperature is occurring purely by a quantum tunneling phenomenon. Complex **5** tunnels between the $M_s = -8$ and $M_s = +8$ levels at a rate of approximately 1×10^{-4} s^{-1}.

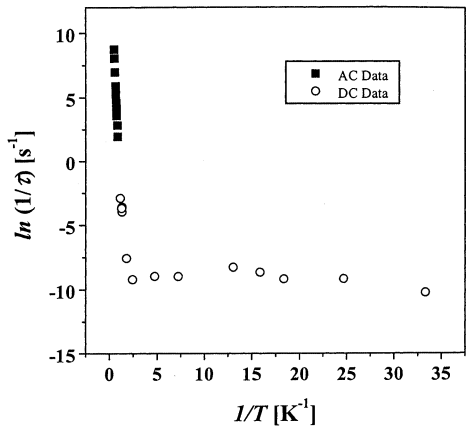

Fig. 9. Plot of the natural logarithm of the relaxation rate ($1/\tau$) versus the inverse absolute temperature for complex **5**. The symbol ■ represents the data collected with the ac magnetic susceptibility technique, and the magnetization decay data are indicated by the symbol O.

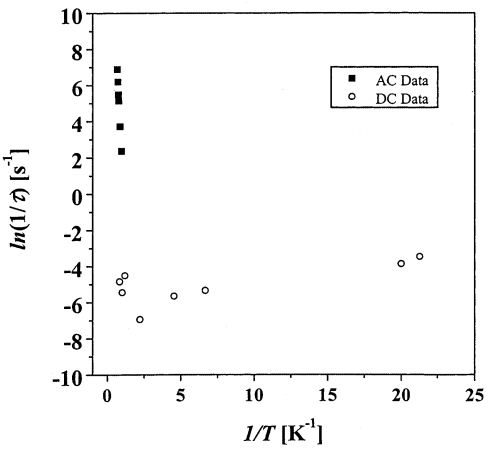

Fig. 10. Plot of the natural logarithm of the relaxation rate ($1/\tau$) versus the inverse absolute temperature for complex **6**. The symbol ■ represents the data collected with the ac magnetic susceptibility technique, and the magnetization decay data are indicated by the symbol O.

Magnetization relaxation decay data were also collected for a sample of complex **6** in the 0.047–1.195 K range. This complex has a $S = 9$ ground state. The decay data were least-squares fit to give relaxation rates in the above temperature range. These rates were combined with those obtained at higher temperatures by means of the ac susceptibility technique and are given in Fig. 10 as an Arrhenius plot. At higher temperatures, the relaxation rate is temperature dependent with an activation energy of 15.8 K. At lower temperatures, we again see a temperature-independent rate of relaxation. This is surely attributable to ground state magnetization tunneling. The temperature-independent magnetization tunneling rate is 1×10^{-3} s^{-1} for complex **6**. Preliminary HFEPR data indicate that complex **6** experiences a larger rhombic zero-field splitting than does complex **5**. This would explain the faster rate of tunneling in complex **6**.

Further experimentation is needed on these interesting tetranuclear manganese SMM's to understand in detail the mechanism of magnetization tunneling in these complexes.

Acknowledgements

D.N.H. and G.C. thank the National Science Foundation for support of this research.

References

[1] R. Sessoli, D. Gatteschi, A. Caneschi, M. Novak, Nature 365 (1993) 149.
[2] R. Sessoli, H.-L. Tsai, A.R. Schake, S. Wang, J.B. Vincent, K. Folting, D. Gatteschi, G. Christou, D.N. Hendrickson, J. Am. Chem. Soc. 115 (1993) 1804.
[3] S.M.J. Aubin, M.W. Wemple, D.M. Adams, H.-L. Tsai, G. Christou, D.N. Hendrickson, J. Am. Chem. Soc. 118 (1996) 7746.
[4] T. Lis, Acta Crystallogr. Sect. B 36 (1980) 2042.
[5] G. Aromí, S.M.J. Aubin, M.A. Bolcar, G. Christou, H.J. Eppley, K. Folting, D.N. Hendrickson, J.C. Huffman, R.C. Squire, H.-L. Tsai, S. Wang, M.W. Wemple, Polyhedron 17 (1998) 3005.
[6] D. Gatteschi, R. Sessoli, A. Cornia, Chem. Commun. (2000) 725.
[7] P.D.W. Boyd, Q. Li, J.B. Vincent, K. Folting, H.-R. Chang, W.E. Streib, J.C. Huffman, G. Christou, D.N. Hendrickson, J. Am. Chem. Soc. 110 (1988) 8537.
[8] A. Caneschi, D. Gatteschi, R. Sessoli, A.L. Barra, L.C. Brunel, M. Guillot, J. Am. Chem. Soc. 113 (1991) 5873.
[9] D. Gatteschi, A. Caneschi, L. Pardi, R. Sessoli, Science 265 (1994) 1054.
[10] A.L. Barra, A. Caneschi, D. Gatteschi, R. Sessoli, J. Am. Chem. Soc. 117 (1995) 8855.
[11] M.A. Novak, R. Sessoli, A. Caneschi, D. Gatteschi, J. Magn. Magn. Mater. 146 (1995) 211.
[12] B. Barbara, W. Wernsdorfer, L.C. Sampaio, J.G. Park, C. Paulsen, M.A. Novak, R. Ferre, D. Mailly, R. Sessoli, A. Caneschi, K. Hasselbach, A. Benoit, L. Thomas, J. Magn. Magn. Mater. 140–144 (1995) 1825.
[13] A.L. Burin, N.V. Prokof'ev, P.C.E. Stamp, Phys. Rev. Lett. 76 (1996) 3040.
[14] R. Politi, A. Rettori, F. Hartmann-Boutron, J. Villain, Phys. Rev. lett. 76 (1996) 3041.
[15] B. Schwarzschile, Phys. Today January 17 (1997).
[16] F. Lionti, L. Thomas, R. Ballou, B. Barbara, A. Sulpice, R. Sessoli, D. Gatteschi, J. Appl. Phys. 81 (1997) 4608.
[17] J.R. Friedman, M.P. Sarachik, J.M. Hernandez, X.X. Zhang, J. Tejada, E. Molins, R. Ziolo, J. Appl. Phys. 81 (1997) 3978.
[18] J.M. Hernandez, X.X. Zhang, F. Luis, J. Tejada, J.R. Friedman, M.P. Sarachik, R. Ziolo, Phys. Rev. B 55 (1997) 5858.
[19] F. Luis, J. Bartolome, J.F. Fernandez, Phys. Rev. B 57 (1998) 505.
[20] M.R. Pederson, S.N. Khanna, Phys. Rev B 59 (1999) 693.
[21] Y. Zhong, M.P. Sarachik, J.R. Friedman, R.A. Robinson, T.M. Kelley, H. Hakotte, A.C. Christianson, F. Trouw, S.M.J. Aubin, D.N. Hendrickson, J. App. Phys. 85 (1999) 5636.
[22] M.N. Leuenberger, D. Loss, Europhys. Lett. 46 (1999) 692.

[23] J.R. Friedman, M.P. Sarachik, J. Tejada, J. Maciejewski, R. Ziolo, J. Appl. Phys. 79 (1996) 6031.
[24] J.R. Friedman, M.P. Sarachik, J. Tejada, R. Ziolo, Phys. Rev. Lett. 76 (1996) 3830.
[25] L. Thomas, F. Lionti, F.R. Ballou, D. Gatteschi, R. Sessoli, B. Barbara, Nature 383 (1996) 145.
[26] J. Tejada, R.F. Ziolo, X.X. Zhang, Chem. Mater. 8 (1996) 1784.
[27] G. Christou, D. Gatteschi, D.N. Hendrickson, R. Sessoli, M.R.S. Bull. 25 (2000) 66.
[28] T. Sala, M.V.J. Sargent, J. Chem. Soc., Chem. Commun. (1978) 253.
[29] S.M.J. Aubin, N.R. Dilley, L. Pardi, J. Krzystek, M.W. Wemple, L.-C. Brunel, M.B. Maple, G. Christou, D.N. Hendrickson, J. Am. Chem. Soc. 120 (1998) 4991.
[30] J. Yoo, E.K. Brechin, A. Yamaguchi, M. Nakano, J.C. Huffman, A.L. Maniero, L.-C. Brunel, K. Awaga, H. Ishimoto, G. Christou, D.N. Hendrickson, Inorg. Chem. 39 (2000) 3615.
[31] J. Yoo, E.K. Brechin, A. Yamaguchi, M. Nakano, J.C. Huffman, A.L. Maniero, L.-C. Brunel, K. Awaga, H. Ishimoto, G. Christou, D.N. Hendrickson, Inorg. Chem. 39 (2000) 3615.
[32] S.M.J. Aubin, Z. Sun, H.J. Eppley, E.M. Rumberger, I.A. Guzei, K. Folting, P.K. Gantzel, A.L. Rheingold, G. Christou, D.N. Hendrickson, Inorg. Chem., in press.
[33] E.M. Chudnovsky, J. Tejada, Macroscopic Quantum Tunneling of the Magnetic Moment, Cambridge University Press, Cambridge, 1998.
[34] A. Caneschi, D. Gatteschi, C. Sangregorio, R. Sessoli, L. Sorace, A. Cornia, M. Novak, C. Paulsen, W. Wernsdorfer, J. Magn. Magn. Mater. 200 (1999) 182.
[35] A.D. Kent, Y. Zhong, L. Bokacheva, D. Ruiz, D.N. Hendrickson, M.P. Sarachik, Europhys. Lett. 49 (2000) 521.
[36] C. Sangregorio, T. Olin, C. Paulsen, R. Sessoli, D. Gatteschi, Phys. Rev. Lett. 78 (1997) 4645.